Skyrmion-induced bound state in a superconductor

Sergey S. Pershoguba[1], Sho Nakosai[1,2], and Alexander V. Balatsky[1,3]
[1]*Nordita, Center for Quantum Materials, KTH Royal Institute of Technology, and Stockholm University, Roslagstullsbacken 23, S-106 91 Stockholm, Sweden*
[2]*Department of Applied Physics, University of Tokyo, Tokyo 113-8656, Japan and*
[3]*Institute for Materials Science, Los Alamos National Laboratory, Los Alamos, New Mexico 87545, USA*
(Dated: October 15, 2015)

We consider a superconductor proximity coupled to a 2D ferromagnetic film with a skyrmionic configuration of a ferromagnetic vector. Using the T-matrix calculations as well as numerical modeling we calculate the spin-polarized local density of states (SP LDOS) in the vicinity of the skyrmion. We identify a skyrmion bound state (SBS) calculate its energy and a spectral width. The SBS resonance has a long-range power-law decay in space. This implies that superconductivity could facilitate a long-range interaction between distinct skyrmions on the surface of a ferromagnetic film.

PACS numbers:

Introduction.— Skyrmions, particle-like topological configurations of a continuous field, were originally proposed in the context of high-energy physics. Nevertheless, it was suggested theoretically [1, 2] and recently observed experimentally [3–7] that skyrmions exist in chiral ferromagnets in the presence of Dzyaloshinkii-Moriya interaction, which is allowed when inversion symmetry is broken. The skyrmions in ferromagnetic films hold great promise in spintronic applications. Due to nontrivial topological properties of skyrmions, they manifest anomalous response to temperature gradients [8] and electric field [9]. Recently, Hamburg group demonstrated controllable writing and deleting of single skyrmions on the surface of PdFe bilayer [10–12].Coupling of magnetic films with skyrmions to novel materials holds a new promising avenue. Coupling of skyrmion to a topological insulator was considered in Ref. [13]. These developments show that skyrmions hold great promise in applications such as spintronics, memory devices, etc [14, 15].

In parallel, there has been a considerable amount of interest recently in ferromagnet-superconductor heterostructures aimed at engineering topological superconductors [16]. Discovery of such topological superconductiviy entails existence of Majorana edge modes in these systems, which would pave the way to realizing topological quantum computing [17]. So, motivated by the immense interest in ferromagnetic skyrmions and the ferromagnet-superconductor heterostructures, we bridge the connection between the two fields in the current paper and study a superconductor prixiimity-coupled to a thin film with a skyrmionic configuration of a ferromagnetic vector as illustrated in Fig. 1. Few works have considered skyrmions in the context of superconductivity. Reference [18] studied the skyrmion-defects in the multiband superfluids and superconductors. A closely related work [19] discussed a possibility of realizing a topological superconductor using a skyrmionic lattice. The Josephson current through a magnetic skyrmion structure was considered in Ref. [20]. However, none of the papers considered the conceptually simplest case of interaction between a single skyrmion and a superconductor, which is discussed in the current work.

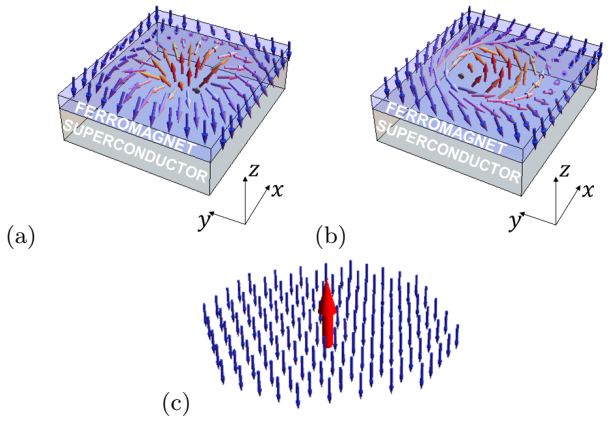

FIG. 1. (Color online.) (a,b) Ferromagnetic film with a skyrmion proximity coupled to a superconductor. (a) Néel-type (hedgehog) skyrmion. (b) Bloch-type (spiral) skyrmion. (c) Sketch of an approximate view of a skyrmion as a local magnetic moment floating in a "ferromagnetic sea".

In the current paper we consider a ferromagnetic film with a skyrmion proximity coupled to a superconductor as shown in Fig. 1. We study a state induced by a skyrmion in a superconductor. In a close analogy with the Yu-Shiba-Rusinov [21–24] states, we find a skyrmion bound state (SBS), a state localized around a skyrmion, using an analytical T-matrix calculation as well as the numerical modeling. The energy of SBS typically lies in between the superconducting bands corresponding to the delocalized states of the opposite spin-polarization. Since skyrmion is a complex object with spins in all directions the spin-up and spin-down sectors of the Hamiltonian are coupled, and SBS is a resonance with a finite spectral width. We calculate a spin-polarized local density of states (SP LDOS) in the vicinity of skyrmions that could be measured using spin-polarized scanning tuneling micropscopy (SP STM) [10–12]. In contrast, with the conventional YSR states, the SBS state is a long-ranged state with a powerlaw decay. Therefore, in the presence

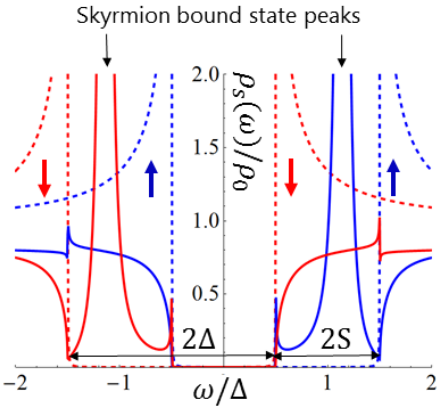

FIG. 2. (Color online) Spin-polarized local density of states (SP LDOS) of a superconductor away from the skyrmion (dashed) and at the skyrmion core (solid). The color of the curves encodes the spin polarization: blue for spin up and red for spin down as indicated by the arrows. The figure is obtained by using a model given by Eqs. (12) and (13) for the parameters $2S = \Delta = 0.1\mu$, $R = 2.5/p_F$, $S_0 = 5SR^2$, and $S_1 = 0.5SR^3$.

of a second skyrmion, the SBS states will interact and give a strong [25] long-ranged "Casimir" interaction [26] between the skyrmions.

Skyrmions in a ferromagnetic film.— Consider a ferromagnetic film with the magnetization described by a three-dimensional vector $\boldsymbol{S}(\boldsymbol{r}) = (S_x, S_y, S_z)$ dependent on a two-dimensional spatial coordinate $\boldsymbol{r} = (x, y)$. The topological configurations of the field $\boldsymbol{S}(\boldsymbol{r})$ shown in Fig. 1(a) and (b) are referred to as skyrmions. Depending on a specific ferromagnetic material, two disctinct types of skyrmions are observed in experiment: the Néel (hedgehog) skyrmion and Bloch (spiral) skyrmion shown in Fig. 1(a) and (b), respectively. The skyrmions observed in experiment vary greatly in size ranging roughly from 10 nm to 1 μm [3–7, 10–12, 27–29]. Although, the two types of skyrmions differ significantly in the orientation of the in-plane spins both are characterized by the same topological charge

$$Q = \frac{1}{4\pi}\int d^2r\, \hat{\boldsymbol{S}}\cdot(\nabla_x\hat{\boldsymbol{S}}\times\nabla_y\hat{\boldsymbol{S}}) = 1, \quad \hat{\boldsymbol{S}} = \frac{\boldsymbol{S}}{S}. \tag{1}$$

Thus, one could continuously transform a Neel skyrmion into a Bloch skyrmion by a mental $\pi/2$ rotation of the ferromagnetic vector around the $\hat{\boldsymbol{z}}$ axis in the spin space without changing a topological charge (1). It would be intriguing to have materials that could exhibit a tunable transition between the two distinct types of skyrmions.

Superconductor proximity coupled to a ferromangetic film.— Let us consider a heterostructure of a ferromagnetic film with a skyrmion deposited on a superconductor as shown in Fig. 1. The superconductor is described by the following 4-by-4 Bogolyubov-de Gennes (BdG) Hamiltonian

$$H = \xi(\boldsymbol{p})\tau_z + \Delta\tau_x - \boldsymbol{S}(\boldsymbol{r})\cdot\boldsymbol{\sigma}, \tag{2}$$

$$\xi(\boldsymbol{p}) = \frac{p^2}{2m} - \mu, \quad \boldsymbol{p} = -i(\nabla_x, \nabla_y). \tag{3}$$

Here, $\xi(\boldsymbol{p})$ describes the kinetic energy and Δ - the self-consistent supeconducting gap, which we assume uniform in space; the term $\boldsymbol{S}(\boldsymbol{r})\cdot\boldsymbol{\sigma}$ represents the proximity coupling between the ferromagnetic film and superconductor. We assume that the Zeeman splitting $S(\boldsymbol{r})$ does not exceed the superconducting gap Δ. The Pauli matrices $\boldsymbol{\tau}$ and $\boldsymbol{\sigma}$ act, respectively, in the particle-hole and spin subspaces of the four-component spinor $\Psi = (\psi_\uparrow, \psi_\downarrow, \psi_\downarrow^\dagger, -\psi_\uparrow^\dagger)^T$. We consider a case with a single Néel skyrmion in the center, and, so, assume the following profile of the ferromagnetic vector

$$\boldsymbol{S}(\boldsymbol{r}) = S\left[\cos\phi(\boldsymbol{r})\sin\theta(\boldsymbol{r}),\, \sin\phi(\boldsymbol{r})\sin\theta(\boldsymbol{r}),\, \cos\theta(\boldsymbol{r})\right],$$
$$\phi(\boldsymbol{r}) = \arctan(y/x), \quad \theta(\boldsymbol{r}) = \pi\left[1 - \exp\left(-\frac{r^2}{R^2}\right)\right], \tag{4}$$

where R defines an effective radius of a skyrmion. The ferromagnetic vector varies from $\boldsymbol{S}(0) = S\hat{\boldsymbol{z}}$ in the center of the skyrmion to $\boldsymbol{S}(\infty) = -S\hat{\boldsymbol{z}}$ away from the skyrmion. Note that for the case of a spin-singlet superconductor given by Eq. (2), the Bloch and the Neel skyrmions are equivalent since they can be related by a continuous $\pi/2$-rotation around the z-axis in the spin space $U = \exp(-i\pi\sigma_z/4)$. In the presence of either the spin-triplet pairing or the spin-orbit interaction the effect of the two types of skyrmions will be different. We focus on the spin-singlet superconductivity, and, thus, the results for the Néel and Bloch skyrmions will coincide. Now let us compare the relevant spatial scales of the problem: the superconducting coherence length $\xi_{\rm sc} \approx v_F/\Delta$, the skyrmion radius R, and the Fermi length p_F^{-1}. Both the superconducting coherence length $\xi_{\rm sc}$ and skyrmion radius can vary greatly in size from few nanometers to a micron depending on a material, whereas the Fermi length p_F^{-1} is typically smaller than the other two scales. Let us first comment on the possible regime of the large skyrmion radius, i.e. $R \gg \xi_{\rm sc}$. In this case, the skyrmion can be viewed as a large ferromagnetic domain pointing in the direction opposite to the rest of the system. Such a case could be intriguing in the context of topological superconductivity [16]. For instance, it was recently pointed out [30] that a helical texture of spins in a one-dimensional chain of magnetic atoms on a surface of a superconductor generates an effective Rashba-like spin-orbit interaction responsible for the Majorana edge modes. Similar effective spin-orbit interaction is generated near a skyrmion and could give rise to non-trivial edge states localized at the edge of the skyrmion. We leave the discussion of this intriguing scenario to future works. In the current paper, we focus on the case of relatively small skyrmions, i.e. $R \leq \xi_{sc}$.

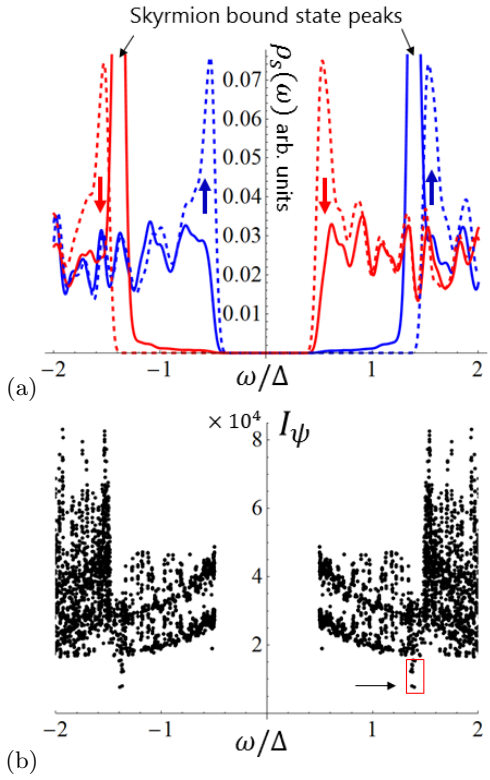

FIG. 3. (Color online) Numerical modeling of a skyrmion. (a) Spin-polarized LDOS at the skyrmion core (solid) and away from the skyrmion (dashed). (b) Participation ratio representing a measure of localization of the BdG wavefunctions. The wavefunctions corresponding to the red dots are shown in Fig. 4 in the panels indicated by the letters.

We search for the possible eigenstates of Hamiltonian (2) localized around a skyrmion in a series of approximations. First we consider a limit of a small skyrmion, i.e. $R \ll \xi_{\rm sc}$, in which case we approximate the skyrmion as a point magnetic moment. Using this simplified model, we do an analytical T-matrix calculation and find peaks in LDOS corresponding to the skyrmion bound state (SBS). Later, we relax the requirement $R \ll \xi_{sc}$ and calculate LDOS and the wavefunction for $R \sim \xi_{sc}$ numerically.

Skyrmion as a local magnetic moment.— Let us consider a case of a small skyrmion, i.e. $R \ll \xi_{\rm sc}$. In this limit, the superconductivity cannot "resolve" the fine details of the field $\boldsymbol{S}(\boldsymbol{r})$. Therefore, we approximate the original skyrmion configuration (4) as a point magnetic moment floating in a "ferromagnetic sea" as illustrated in Fig. 1(c)

$$\boldsymbol{S}_{\rm approx}(\boldsymbol{r}) = -S\hat{\boldsymbol{z}} + S_0\hat{\boldsymbol{z}}\delta^2(\boldsymbol{r}), \tag{5}$$

where S_0 is defined via the original skyrmion configuration (4)

$$S_0 = \int d^2r\ \left[\boldsymbol{S}(\boldsymbol{r}) - \boldsymbol{S}(\infty)\right]_z \quad \sim \quad SR^2. \tag{6}$$

Formally, the approximation given by Eqs. (5) and (6) is justified when the skyrmion $R < p_F^{-1}$, since it assumes that the scattering potential is sharp enough to provide the momenta connecting different k-points on the Fermi surface.

By performing the T-matrix calculation, we solve the model given by Eqs. (2) and (5), where we treat the local term $S_0\hat{\boldsymbol{z}}\delta^2(\boldsymbol{r})$ as a perturbation. We include the constant background magnetization $-S\hat{\boldsymbol{z}}$ in the BdG Hamiltonian $h(\boldsymbol{p}) = \xi(\boldsymbol{p})\tau_z + \Delta\tau_x + S\sigma_z$ and calculate an on-site matrix element of the bare Green's function $g(\omega, \boldsymbol{p}) = [\omega - h(\boldsymbol{p})]^{-1}$

$$g_0(\omega) = -\pi\rho \sum_{\lambda=\pm1} \frac{1+\lambda\sigma_z}{2} \frac{\omega - \lambda S + \Delta\tau_x}{\sqrt{\Delta^2 - (\omega - \lambda S)^2}}, \tag{7}$$

where $\rho = m/2\pi$ is the density of states. This Green's function describes a superconductor subject to a uniform background magnetization $-\hat{\boldsymbol{z}}S$ and gives a spin-polarized local density of states (SP LDOS) shown by dashed lines in Fig. 2. The density of states contains two inside coherence peaks at the energies $\pm(\Delta - S)$, and two outside - at the energies $\pm(\Delta + S)$. So, the spectra for the spin-up and spin-down sectors of the Hamiltonian, plotted in blue and red, are shifted relatively by $2S$. Using Green's function (7) we calculate the T-matrix in the presence of a point magnetic moment $V(\boldsymbol{r}) = S_0\,\sigma_z\delta^2(\boldsymbol{r})$ representing the skyrmion

$$T(\omega) = \frac{-S_0\sigma_z}{1 + S_0\sigma_z g_0(\omega)}. \tag{8}$$

The poles of T-matrix give the new skyrmion-induced bound states (SBS). To find their energy we find the roots of the equation $\det\left[1 + S_0\sigma_z g_0(\omega)\right] = 0$

$$E^{\pm}_{\rm SBS} = \pm\left[S + \Delta\frac{1 - (\pi\rho S_0)^2}{1 + (\pi\rho S_0)^2}\right]. \tag{9}$$

Let us mention the behavior of the SBS peaks as a function of S_0. For small S_0, the SBS states split from the outside coherence peaks at the energies $\pm(\Delta + S)$ and move in the direction of the inside coherence peaks with a further increase of S_0. Although Eq. (9) suggests that the SBS states may go inside the actual gap for large enough S_0, i.e. $|E^{\pm}_{\rm SBS}| < \Delta - S$, the approximation of a skyrmion (5) is no-longer valid in this regime and, thus, does not give a reliable estimate of the SBS energy. In practice, by performing a numerical modeling discussed below, we never observe the SBS peaks inside the actual band gap, i.e. beyond the energies $|E^{\pm}_{\rm SBS}| > \Delta - S$. The spin-polarization of the SBS states is determined by the spin-polarization of the bulk bands that they split from: the positive (negative) SBS state is "up" ("down") spin-polarized. The found SBS states closely mimic the well-known Yu-Shiba-Rusinov (YSR) states [21–24] localized around magnetic impurities in superconductors. The main difference is that the YSR states'

energies reside inside the actual spectral gap, whereas the SBS states' energies lie in the window of energies $\Delta + S > |E^{\pm}_{\rm SBS}| > \Delta - S$. So, the SBS states could hybridize with the bands of the opposite spin polarization.

Indeed, so far we have considered an approximation of a skyrmion given by Eq. (5) that includes only σ_z matrices. In this approximation, the spin-up and spin-down sectors of the Hamiltonian are decoupled. However let us recall that the original configuration of a ferromagnetic vector in a skyrmion (4) has spins in all directions. Specifically, the ferromagnetic vector $\boldsymbol{S}(\boldsymbol{r})$ given by Eq. (4) is purely in-plane for $r = R\sqrt{\ln 2}$. Such in-plane moments generate the terms proportional to σ_x and σ_y in the Hamiltonian that could couple the spin-up and spin-down sectors of the Hamiltonian. To capture this effect we append the approximation (5) with an additional term

$$\boldsymbol{S}_{\rm approx}(\boldsymbol{r}) = -S\hat{\boldsymbol{z}} + S_0\hat{\boldsymbol{z}}\delta^2(\boldsymbol{r}) - S_1\boldsymbol{\nabla}\delta^2(\boldsymbol{r}), \qquad (10)$$

where $\boldsymbol{\nabla} = (\nabla_x, \nabla_y)$ and S_1 is the first-moment of the original skyrmion configuration[31]

$$S_1 = \frac{1}{2}\int d^2r\ [\boldsymbol{S}(\boldsymbol{r}) - \boldsymbol{S}(\infty)]\cdot\boldsymbol{r} \quad \sim \quad SR^3. \qquad (11)$$

Indeed, the last term in (10) mimicks the radial in-plane spins of the skyrmion. Similar to calculation above, we solve the Lippmann-Schwinger equation (see details in Supplementary Materials) and calculate the T-matrix

$$T(\omega) = \frac{-S_0\sigma_z + S_1^2 p_F^2\,\bar{g}_0(\omega)}{1 + S_0\sigma_z g_0(\omega) - S_1^2 p_F^2\,\bar{g}_0(\omega)\,g_0(\omega)}, \qquad (12)$$

where for brevity $\bar{g}_0(\omega) = \frac{1}{2}\sum_{j=x,y}\sigma_j g_0(\omega)\sigma_j$ is the Green's function obtained from Eq. (7) by substitution $\sigma_z \to -\sigma_z$, that describes the coupling to bands with opposite spin polarization. Using Eq. (12) we calculate SP LDOS

$$\rho_s(\omega) = \qquad (13)$$
$$-\frac{1}{\pi}\,{\rm Im\,Tr}\left\{\frac{1+\tau_z}{2}\,\frac{1+\sigma_s}{2}\,[g_0(\omega) + g_0(\omega)T(\omega)g_0(\omega)]\right\},$$

where the energy has infinitesimally small imaginary part in the right side of the equation, i.e. $\omega \to \omega + i\delta$, and $s = x, y, z$ denotes the spin projection axis. We plot LDOS (13) in Fig. 2 with solid lines and observe that the peaks corresponding to the SBS resonances have finite spectral width. In order to understand this, we compare Eqs. (8) and (12) and observe that the latter contains renormalized numerator and the denominator due to S_m. Let us consider poles of the T-matrix (12) given by $\det\left[1 + S_{\rm e}\sigma_z g_0(\omega) - S_{\rm m}^2 p_F^2\,\bar{g}_0(\omega)\,g_0(\omega)\right] = 0$. The real part of this equation still gives the SBS state given by Eq. (9). However, since $\bar{g}_0(\omega)$, which is the Green's function for a flipped spin, is imaginary at the SBS energy, the term $S_{\rm m}^2 p_F^2\,\bar{g}_0(\omega)\,g_0(\omega)$ becomes imaginary and determines a finite spectral width of SBS resonance. This

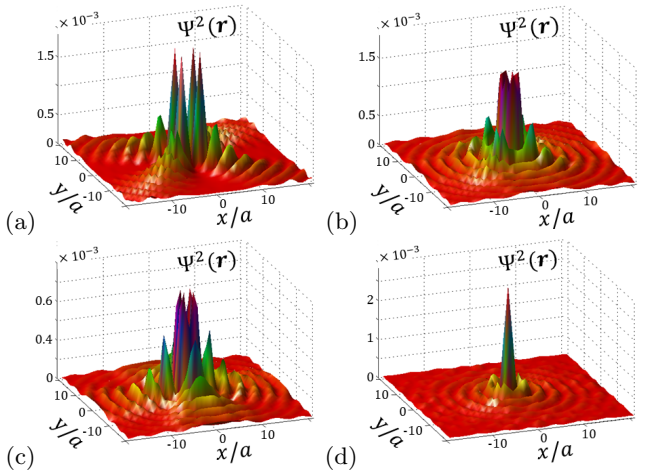

FIG. 4. (Color online) Spatial profile of the quasilocalized wavefunctions obtained numerically, which are indicated in Fig. 3(b).

explains the apparent widening of the spectrum around the SBS state. Figure (2) allows to compare SP LDOS at the skyrmion core, shown with solid lines, and the energy spectrum far from a skyrmion, shown with dashed lines.

Long-range wave function Now let us show that the wave function corresponding to the SBS state has a long-range power-law behavior. Generically, the wave function of an impurity induced state is described by the wave function

$$\Psi(\boldsymbol{r}) \sim \frac{e^{ip_F r}e^{-r\sqrt{\Delta^2-\omega_\lambda^2}/v_F}}{\sqrt{r}}, \qquad (14)$$

where for brevity λ denotes the eigenvalues of σ_z operator and $\omega_\lambda = \omega - \lambda S$. The former exponential term in Eq. (14) describes the fast Friedel oscillations, whereas latter term - behavior at a scale of superconducting coherence length. For clarity, let us discuss the positive SBS state, i.e. $\omega = E^{+}_{\rm SBS}$. It lies inside the superconducting gap for the spin-up subsystem, i.e. $\omega_+ < \Delta$, and, so, the latter exponential term in Eq. (14) describes the exponentially decaying behavior. However, the SBS state also couples to the background spin-down delocalized band, for which it is supragap state, i.e. $\omega_- > \Delta$. Therefore, the square root in the Eq. (14) becomes imaginary $\sqrt{\Delta^2 - \omega_-^2} = -i\sqrt{\omega_-^2 - \Delta^2}$, and, so, Eq. (14) describes the oscillating behavior at a scale ξ_{sc}. In colloquial terms, the exponentially localized YSR state hybridizes with the delocalized states and produces a long-range SBS state.

Numerical analysis.— So, approximating a skyrmion as a point impurity, which is valid if $R \ll \xi_{sc}$, we showed that the skyrmion induces resonances in LDOS. We now relax a requirement of small skyrmions and numerically calculate SP LDOS for a large skyrmion $R \sim \xi$. We put the BdG Hamiltonian onto a 2D square lattice with 200-by-200 sites and numerically diagonalize it. The parameters of the tight binding Hamiltonian are $0.1t = \Delta = 2S$,

$\mu = -3t$, t is a nearest neighbour tunneling amplitude; the radius of skyrmion $R = 6a$, where a is a lattice constant. We numerically calculate SP LDOS and show it in Fig. 3(a). We use the same style as Fig. 2: solid (dashed) line represents LDOS on (away from) skyrmion, colors encode opposite spin polarizations. We observe that the calculate LDOS is consistent with the discussion above. Skyrmion does induce a resonance in the LDOS in the energy window in between the original spin-split bands. We also look at the individual normalized BdG eigenstates and calculate the participation ratio

$$I_\psi = \sum_{\boldsymbol{r}} |\psi(r)|^4, \tag{15}$$

where the sum is carried over lattice sites $\boldsymbol{r}$. The participation ratio measures a degree of a localization of a wavefunctions: for a localized wavefunction $I_\psi \approx 1$ and for delocalized $I_\psi \approx N$, where $N = 200^2$ is the size of the system. We map I_ψ for all numerical eigenstates and find quasilocalized states for energies corresponding to the SBS peak. We show the electron part $|u_\uparrow|^2 + |u_\downarrow|^2$ of the corresponding wavefunction in Fig. 4. We observe that the states with different angular momenta fill up the SBS peak.

Conclusion and Outlook.— In this paper, we predict a new skyrmion bound state (SBS) in a superconductor proximity coupled to a ferromagnetic film with a skyrmion. We calculate SP LDOS and show the signatures of SBS in the tunneling spectrum. The skyrmion typically induces a resonance in between the spin-split coherence peaks corresponding to the opposite spin polarizations. We show that the wavefunction of SBS is quasilocalized, i.e. decays as $1/\sqrt{r}$. Thus in the case of the two skyrmions, their SBS wavefunctions will overlap and induce a long-range interaction between skyrmions [25, 32]. This will be explored in a following publication.

We hope that the current paper will be a first step in studying superconductor-skyrmionic heterostructures and motivate further experimental and theoretical research. There are intriguing questions in this direction. For instance, superconductivity could in induce effective Dzyaloshinkii-Moriya especially for non-centrosymmetric materials and, thus, stabilize the skyrmionic phase. It would be interesting to explore the connection with the topological superconductivity hybrid systems [16]. Superconductivity could potentially endow the skyrmion with a non-trivial statistics by captivating a Majorana fermion.

We thank R. Wiesendanger, Fujimoto, J. Zang, A. Saxena for useful discussions. This work was supported by the US DOE BES E304, ERC DM-321031 and KAW (S.S.P. and A.V.B.).

[1] A. N. Bogdanov and D. A. Yablonskii, "Thermodynamically stable "vortices" in magnetically ordered crystals. The mixed state of magnets." Sov. Phys. JETP **68**, 101 (1989).

[2] U K Rössler, A N Bogdanov, and C Pfleiderer, "Spontaneous skyrmion ground states in magnetic metals." Nature **442**, 797 (2006).

[3] S Mühlbauer, B Binz, F Jonietz, C Pfleiderer, A Rosch, A Neubauer, R Georgii, and P Böni, "Skyrmion lattice in a chiral magnet." Science **323**, 915 (2009).

[4] W. Münzer, A. Neubauer, T. Adams, S. Mühlbauer, C. Franz, F. Jonietz, R. Georgii, P. Böni, B. Pedersen, M. Schmidt, A. Rosch, and C. Pfleiderer, "Skyrmion lattice in the doped semiconductor $Fe_{1-x}Co_xSi$," Phys. Rev. B **81**, 041203 (2010).

[5] X. Z. Yu, N. Kanazawa, Y. Onose, K. Kimoto, W. Z. Zhang, S. Ishiwata, Y. Matsui, and Y. Tokura, "Near room-temperature formation of a skyrmion crystal in thin-films of the helimagnet FeGe," Nat. Mater. **10**, 106 (2011).

[6] Stefan Heinze, Kirsten von Bergmann, Matthias Menzel, Jens Brede, Andre Kubetzka, Roland Wiesendanger, Gustav Bihlmayer, and Stefan Blugel, "Spontaneous atomic-scale magnetic skyrmion lattice in two dimensions," Nat Phys **7**, 713–718 (2011).

[7] S. Seki, X. Z. Yu, S. Ishiwata, and Y. Tokura, "Observation of Skyrmions in a Multiferroic Material," Science **336**, 198 (2012).

[8] F. Jonietz, S. Mhlbauer, C. Pfleiderer, A. Neubauer, W. Mnzer, A. Bauer, T. Adams, R. Georgii, P. Bni, R. A. Duine, K. Everschor, M. Garst, and A. Rosch, "Spin Transfer Torques in MnSi at Ultralow Current Densities," Science **330**, 1648 (2010).

[9] A. Neubauer, C. Pfleiderer, B. Binz, A. Rosch, R. Ritz, P. G. Niklowitz, and P. Böni, "Topological Hall Effect in the A Phase of MnSi," Phys. Rev. Lett. **102**, 186602 (2009).

[10] N. Romming, C. Hanneken, M. Menzel, J. E. Bickel, B. Wolter, K. von Bergmann, A. Kubetzka, and R. Wiesendanger, "Writing and Deleting Single Magnetic Skyrmions," Science **341**, 636 (2013).

[11] K. von Bergmann, A. Kubetzka, O. Pietzsch, and R. Wiesendanger, "Interface-induced chiral domain walls, spin spirals and skyrmions revealed by spin-polarized scanning tunneling microscopy," J. Phys.: Condens. Matter **26**, 394002 (2014).

[12] N. Romming, A. Kubetzka, C. Hanneken, K. von Bergmann, and R. Wiesendanger, "Field-Dependent Size and Shape of Single Magnetic Skyrmions," Phys. Rev. Lett. **114**, 177203 (2015).

[13] Hilary M. Hurst, Dmitry K. Efimkin, Jiadong Zang, and Victor Galitski, "Charged skyrmions on the surface of a topological insulator," Phys. Rev. B **91**, 060401 (2015).

[14] Albert Fert, Vincent Cros, and Joao Sampaio, "Skyrmions on the track," Nat. Nano **8**, 152–156 (2013).

[15] N. Nagaosa and Y. Tokura, "Topological properties and dynamics of magnetic skyrmions," Nat. Nanotechnol. **8**, 899 (2013).

[16] Jason Alicea, "New directions in the pursuit of Majorana fermions in solid state systems." Rep. Prog. Phys. **75**,

076501 (2012).
[17] Chetan Nayak, Steven H. Simon, Ady Stern, Michael Freedman, and Sankar Das Sarma, "Non-abelian anyons and topological quantum computation," Rev. Mod. Phys. **80**, 1083–1159 (2008).
[18] Julien Garaud, Johan Carlström, and Egor Babaev, "Topological solitons in three-band superconductors with broken time reversal symmetry," Phys. Rev. Lett. **107**, 197001 (2011).
[19] S. Nakosai, Y. Tanaka, and N. Nagaosa, "Two-dimensional p-wave superconducting states with magnetic moments on a conventional s-wave superconductor," Phys. Rev. B **88**, 180503 (2013).
[20] Takehito Yokoyama and Jacob Linder, "Josephson effect through magnetic skyrmions," Phys. Rev. B **92**, 060503 (2015).
[21] L. Yu, "Bound state in superconductors with paramagnetic impurities," Acta Phys. Sin. **21**, 75 (1965).
[22] H. Shiba, "Classical Spins in Superconductors," Prog. Theor. Phys. **40**, 435 (1968).
[23] A. I. Rusinov, "Superconductivity near a paramagnetic impurity," JETP Lett. **9**, 85 (1969).
[24] A. V. Balatsky, I. Vekhter, and J.-X. Zhu, "Impurity-induced states in conventional and unconventional superconductors," Rev. Mod. Phys. **78**, 373 (2006).
[25] N. Y. Yao, L. I. Glazman, E. A. Demler, M. D. Lukin, and J. D. Sau, "Enhanced Antiferromagnetic Exchange between Magnetic Impurities in a Superconducting Host," Phys. Rev. Lett. **113**, 087202 (2014).
[26] Andrei V. Shytov, Dmitry A. Abanin, and Leonid S. Levitov, "Long-range interaction between adatoms in graphene," Phys. Rev. Lett. **103**, 016806 (2009).
[27] J. Brede, N. Atodiresei, V. Caciuc, M. Bazarnik, A. Al-Zubi, S. Blügel, and R. Wiesendanger, "Long-range magnetic coupling between nanoscale organicmetal hybrids mediated by a nanoskyrmion lattice," Nat. Nanotechnol. **9**, 1018 (2014).
[28] A. Sonntag, J. Hermenau, S. Krause, and R. Wiesendanger, "Thermal Stability of an Interface-Stabilized Skyrmion Lattice," Phys. Rev. Lett. **113**, 077202 (2014).
[29] K. von Bergmann, M. Menzel, A. Kubetzka, and R. Wiesendanger, "Influence of the Local Atom Configuration on a Hexagonal Skyrmion Lattice," Nano Lett. **15**, 3280 (2015).
[30] J. Klinovaja, P. Stano, A. Yazdani, and D. Loss, "Topological superconductivity and majorana fermions in rkky systems," Phys. Rev. Lett. **111**, 186805 (2013).
[31] Note that in the case of the Block skyrmion S_1 would have a physical meaning of an anapole moment defined as $S_1 = \frac{1}{2}\int d^2r\ \{[\boldsymbol{S}(\boldsymbol{r}) - \boldsymbol{S}(\infty)] \times \boldsymbol{r}\}_z$.
[32] G. C. Ménard, S. Guissart, C. Brun, S. Pons, V. S. Stolyarov, F. Debontridder, M. V. Leclerc, E. Janod, L. Cario, D. Roditchev, P. Simon, and T. Cren, "Long range coherent magnetic bound states in superconductors," arXiv:1506.06666.

Appendix A: T-matrix analysis

In this section, we give an analytic treatment of the skyrmion-induced bound states using the T-matrix approximation. Starting from the Hamiltonian (2) in the second-quantized form, we write the Bogolyubov-de Gennes (BdG) Hamiltonian as

$$H_{\rm BdG} = h(\boldsymbol{p}) + V(\boldsymbol{r}), \quad \text{where} \tag{A1}$$
$$H(\boldsymbol{p}) = \xi(\boldsymbol{p})\tau_z + \Delta\tau_x - \boldsymbol{S}(\infty)\cdot\boldsymbol{\sigma}, \quad \boldsymbol{S}(\infty) = -S\,\hat{\boldsymbol{z}},$$
$$V(\boldsymbol{r}) = -\left[\boldsymbol{S}(\boldsymbol{r}) - \boldsymbol{S}(\infty)\right]\cdot\boldsymbol{\sigma} \tag{A2}$$

The momentum-dependent part $H(\boldsymbol{p})$ describes a superconductor coupled to a spatially uniform ferromagnetic vector $\boldsymbol{S}(\infty)$, whereas the position-dependent piece $V(\boldsymbol{r})$ describes the local perturbation due to the skyrmion. Although the specific model is not significant, we assume the following model for the skyrmion centered at the origin $r = 0$

$$\boldsymbol{S}(\boldsymbol{r}) = S\left[\cos\phi(\boldsymbol{r})\sin\theta(\boldsymbol{r}),\ \sin\phi(\boldsymbol{r})\sin\theta(\boldsymbol{r}),\ \cos\theta(\boldsymbol{r})\right],$$
$$\phi(\boldsymbol{r}) = \arctan(x/y), \quad \theta(\boldsymbol{r}) = \pi\left[1 - \exp\left(-\frac{r^2}{R^2}\right)\right], \tag{A3}$$

where $\phi(\boldsymbol{r})$ and $\theta(\boldsymbol{r})$ denote the polar and azimuthal angle of the vector $\boldsymbol{S}(\boldsymbol{r})$, and R controls the skyrmion size. The superconducting coherence length is usually greater than a typical skyrmion size $R \sim 5\,\text{nm}$ [6, 10–12, 27–29], i.e. $\xi_{\rm sc} \gg R$. Therefore, the superconductivity does not "resolve" the fine details of the skyrmionic configuration of the field $\boldsymbol{S}(\boldsymbol{r})$, but rather "sees" its long-wavelength characteristics such as the moments described by Eqs. (6) and (11). Motivated by this logic, we substitute the original skyrmionic field $\boldsymbol{S}(\boldsymbol{r})$ by its local version

$$\boldsymbol{S}(\boldsymbol{r}) - \boldsymbol{S}(\infty) = \left[S_{\rm e}\,\hat{\boldsymbol{z}} - S_{\rm m}\,\boldsymbol{\nabla}\right]\delta^2(\boldsymbol{r}). \tag{A4}$$

Here, in order to relate the moments to the original parameters of the model we subtitute Eq. (A3) in Eqs. (6) and (11) and find

$$S_{\rm e} = SR^2\pi\left[-\mathrm{Ci}(\pi) + \gamma + \log(\pi)\right] \approx 5.18\,SR^2, \tag{A5}$$
$$S_{\rm m} = SR^3\int_0^\infty 2\pi t^2 \sin\left(\pi e^{-t^2}\right)\,dt \approx 6.53\,SR^3. \tag{A6}$$

Equation (A4) is convenient for the T-matrix calculation, which we now proceed to. We take into account (A4) and calculate the Fourier transform of Eq. (A2)

$$V(\boldsymbol{p}) = -S_{\rm e}\,\sigma_z + i\,S_{\rm m}\,\boldsymbol{\sigma}\cdot\boldsymbol{p}, \tag{A7}$$

using which we write an intergal equation for the T-matrix

$$T\left(\boldsymbol{p}^1, \boldsymbol{p}^2\right) = V\left(\boldsymbol{p}^1 - \boldsymbol{p}^2\right) + \int \frac{d^2p'}{(2\pi)^2}\,V\left(\boldsymbol{p}^1 - \boldsymbol{p}'\right)g(\omega, \boldsymbol{p}')T\left(\boldsymbol{p}', \boldsymbol{p}^2\right). \tag{A8}$$

Here, the bare Green's function of the superconductor is defined as

$$g(\omega, \boldsymbol{p}) = \frac{1}{\omega - h(\boldsymbol{p})} = \frac{1}{\omega - \xi(\boldsymbol{p})\tau_z - \Delta\tau_x - S\sigma_z}. \tag{A9}$$

Since in the case of the superconductivity we are interested in the scatterings close to the Fermi surface, we use $\boldsymbol{p}^1 = p_F\,\boldsymbol{n}^1$ and $\boldsymbol{p}^2 = p_F\,\boldsymbol{n}^2$, where the in-plane unit vectors $\boldsymbol{n}^1$ and $\boldsymbol{n}^2$ determine the direction of scattering on the Fermi surface. Then, we seek the T-matrix in the following form

$$T\left(\boldsymbol{n}^1,\boldsymbol{n}^2\right) = A + B_i n_i^1 + C_i n_j^2 + D_{ij} n_i^1 n_j^2, \qquad \text{(A10)}$$

where A, B_i, C_i and D_{ij} are the matrices in the four-components space $\sigma\otimes\tau$. We substitute ansatz (A10) in the integral Eq. (A8) and find the T-matrix

$$T\left(\boldsymbol{n}^1,\boldsymbol{n}^2\right) = \frac{-S_{\rm e}\sigma_z + S_{\rm m}^2 p_F^2 \bar{g}_0(\omega) + i\,S_{\rm m}\,p_F\,\boldsymbol{\sigma}\cdot(\boldsymbol{n}^2-\boldsymbol{n}^1) + S_{\rm m}^2\,p_F^2\,\bar{g}_0(\omega)\,\left(\boldsymbol{\sigma}\cdot\boldsymbol{n}^2\right)\,\left(\boldsymbol{\sigma}\cdot\boldsymbol{n}^1\right)}{1 + S_{\rm e}\sigma_z g_{00} - S_{\rm m}^2 p_F^2\,\bar{g}_0(\omega)\,g_0(\omega)}, \qquad \text{(A11)}$$

where the Green's function on-site matrix element in the real space is denoted as

$$g_0(\omega) = \int \frac{d^2p}{(2\pi)^2}\,g(\omega,\boldsymbol{p}) \qquad \text{(A12)}$$
$$= -\pi\rho \sum_{\lambda=\pm1} \frac{1+\lambda\sigma_z}{2}\,\frac{\omega-\lambda S+\Delta\tau_x}{\sqrt{\Delta^2-(\omega-\lambda S)^2}},$$
$$\bar{g}_0(\omega) = \frac{1}{2}\sum_{j=x,y}\sigma_j\,g_0(\omega)\,\sigma_j. \qquad \text{(A13)}$$

For brevity, $\bar{g}_0$ denotes the Green's function obtained from g_{00} by replacing $\sigma_z \to -\sigma_z$ according to Eq. (A13). The density of states per spin is denoted as $\rho = m/2\pi$. So, in the presence of the skyrmion, the Green's function becomes

$$G(\omega,\boldsymbol{p}^1,\boldsymbol{p}^2) = g(\omega,\boldsymbol{p}^1)\,(2\pi)^2\delta(\boldsymbol{p}^1-\boldsymbol{p}^2) + g(\omega,\boldsymbol{p}^1)T(\boldsymbol{p}^1,\boldsymbol{p}^2)g(\omega,\boldsymbol{p}^2), \qquad \text{(A14)}$$

using which the spin-polarized local density of states (LDOS) can be expressed

$$\rho_s(\omega,\boldsymbol{r}) = -\frac{1}{\pi}\,\mathrm{Im}\lim_{\omega\to\omega+i\delta}\mathrm{Tr}\left[\frac{1+\tau_z}{2}\,\frac{1+\sigma_s}{2}\int\frac{d^2p^1\,d^2p^2}{(2\pi)^4}e^{i(\boldsymbol{p}^1-\boldsymbol{p}^2)\boldsymbol{r}}G(\omega,\boldsymbol{p}^1,\boldsymbol{p}^2)\right] \qquad \text{(A15)}$$

where $s = x, y, z$ denotes the spin quantization axis. It can be easily evaluated for instance at the skyrmion core, i.e. at $\boldsymbol{r} = 0$,

$$\rho_s(\omega,0) = -\frac{1}{\pi}\,\mathrm{Im}\lim_{\omega\to\omega+i\delta}\mathrm{Tr}\left\{\frac{1+\tau_z}{2}\,\frac{1+\sigma_s}{2}\left[g_0(\omega) + g_0(\omega)\frac{-S_{\rm e}\sigma_z + S_{\rm m}^2 p_F^2\bar{g}_0(\omega)}{1+S_{\rm e}\sigma_z g_{00} - S_{\rm m}^2 p_F^2\,\bar{g}_0(\omega)\,g_0(\omega)}g_0(\omega)\right]\right\} \qquad \text{(A16)}$$